Surface-Assembly and Redox Dissolution of Silver Nanoparticles Monitored by Evanescent Wave Cavity Ring-down Spectroscopy

Mathias Schnippering,[1] *Hayley V. Powell,*[1] *Meiqin Zhang,*[1]

Julie V. Macpherson,[1] *Patrick R. Unwin,*[1*]

Mikhail Mazurenka[2] *and Stuart R. Mackenzie*[2*]

[1] Department of Chemistry, University of Warwick, Gibbet Hill Road, Coventry, CV4 7AL, UK.

[2] Department of Chemistry, University of Cambridge, Lensfield Road, Cambridge, CB2 1EW, UK.

September 12, 2019

[*]P.R.Unwin@warwick.ac.uk, tel. + 44 24 7652 3264

[*]srm49@cam.ac.uk

KEYWORDS: silver nanoparticles, evanescent wave cavity ring-down spectroscopy, dissolution kinetics, atomic force microscopy, redox reactions

Abstract

The adsorption kinetics of Ag nanoparticles on a silica surface modified with poly-L-lysine (PLL) have been measured *in situ* by following the interfacial optical absorbance at 405 nm using evanescent wave cavity ring-down spectroscopy (EW-CRDS). Sensitivity towards nanoparticle detection is enhanced due to the plasmon resonance of the Ag nanoparticles. The redox-dissolution kinetics of the immobilized nanoparticles have been investigated using two distinct approaches. First, $IrCl_6^{2-}$ was generated electrochemically from $IrCl_6^{3-}$ by a chronoamperometric potential step in a thin layer cell configuration formed between the silica surface and a Pt macroelectrode. The oxidative dissolution kinetics were obtained by monitoring the EW-CRDS signal as the nanoparticles dissolved. The reaction kinetics were extracted using complementary finite element modeling of diffusional and reaction processes. The second method of dissolution investigated involved the injection of $IrCl_6^{2-}$ (aq) directly at the surface by means of a microcapillary located close to the evanescent field.

Introduction

Immobilized arrays of metal nanoparticles continue to attract considerable attention for electronic and sensing applications,[1-3] including biosensing and the study of protein interactions.[4-8] In the latter context, Ag nanoparticles have proven useful for staining applications, which enables the visualization of proteins and DNA, and as an integral component of antibacterial coatings. Ag nanoparticles can be functionalized with oligonucleotides for DNA sensing applications[9] or act as bridge materials for electron transfer reaction from proteins to electrodes.[10] It has also been shown that Ag nanoparticles can be used as substrates for surface-enhanced Raman scattering (SERS).[11-13]

For these applications, and others, understanding reactions at the nanoscale, especially electron transfer at nanostructures and metal nanoparticles, is very important. The oxidative etching kinetics of metal surfaces were probed in earlier scanning electrochemical microscopy (SECM) work by us[14] using tris(2,2'-bipyridyl)ruthenium(III) and Br_2 as electrogenerated oxidants. Only a few studies have investigated the dissolution of nanoparticles, either in solution by varying the pH[15-17] and through O_2 purging,[18] or embedded in a glass matrix. In the latter case, the particles were dissolved using heat,[19] ultrafast laser pulses[20] or intense electric fields.[21,22] In all these examples, analysis was performed either *ex-situ* or in bulk using conventional UV-vis spectroscopy. To date there have been no time-resolved studies of the dissolution kinetics of metal nanoparticles on insulating surfaces. In order to monitor and rationalize these processes, rather sensitive analytical techniques are needed.

The redox mediator $[IrCl_6]^{3-/4-}$ has been employed in several previous studies to dissolve Ag nanoparticles. For example, it has been applied to protein detection using SECM (generation of $IrCl_6^{2-}$ from $IrCl_6^{3-}$ at an ultramicroelectrode) after Ag staining[23] and for Ag enhanced fingerprint determination.[24] The formation of electrochemically-generated Ag nanoparticles has been investigated by Rodriguez-Sanchez *et al.*[25] In all these studies, the Ag nanoparticle dissolution/growth was either detected indirectly using surface sensitive techniques such as scanning electron microscopy and X-ray scattering or time-resolved by bulk UV-vis spectroscopy. It has not been possible to combine both approaches.

Evanescent Wave - Cavity Ringdown Spectroscopy (EW-CRDS) is rapidly emerging as a highly sensitive technique for the determination of interfacial kinetics, in condensed phase systems.[26-28] Several groups have used EW-CRDS to study the adsorption kinetics of different dyes, as well as biologically interesting molecules, in real time.[26-31] We recently reported the use of EW-CRDS for measurement of gold colloid deposition on poly-L-lysine (PLL)-functionalized silica.[32] The present paper illustrates the use of EW-CRDS as a powerful technique for the study of the kinetics of processes on insulating surfaces such as adsorption and dissolution, which has been challenging in the past because the introduction/removal of the adsorbents into a solution has to occur on a rapid timescale. A key attribute of EW-CRDS is its surface sensitivity which arises due to the small penetration depth (typically ~100 nm) of the evanescent field beyond the boundary of interest. For condensed phases, this opens up a wide range of applications for either adsorption studies or nanoscale reaction kinetics, coupled with an impressive temporal resolution.

In this report, the adsorption of Ag nanoparticles onto PLL-modified silica was investigated, extending the work on other metal nanoparticles reported previously.[33,34] The kinetics were followed in real time, permitting the extraction of key information about the rate controlling processes. This part of the paper highlights the sensitivity of the EW-CRDS technique in probing the assembly of disperse films of particles.

The kinetics of the redox dissolution of Ag colloidal particles were also obtained by combining EW-CRDS with electrochemistry. The nanoparticles were dissolved using the redox compound $IrCl_6^{2-}$ which was electrochemically generated from the reduced (non-reactive) form, $IrCl_6^{3-}$, at a strategically located electrode just above the silica surface. $IrCl_6^{2-}$ oxidizes Ag^0 to Ag^+ causing dissolution of the nanoparticles. Studies were carried out for various concentrations of $IrCl_6^{3-}$ and different electrogeneration times, using a potential step method. The experimental data, in the form of interfacial absorbance-time plots, were used to calculate the rate constant of the dissolution process after solution of the underlying mass transport problem.

A second method of Ag colloid dissolution was also tested, in which a simple micropipette was used to dispense the reagent ($IrCl_6^{2-}$ solution) directly in the region of the immobilized nanoparticles. The dissolution process was followed as a function of $IrCl_6^{2-}$ concentration and flow rate. These initial studies provide a platform for the further use of this technique.

Theory

In order to extract kinetic parameters from the experimental observations, we fitted the data obtained to a simple model, encapsulating the diffusion of the electrogenerated species and the kinetics of dissolution. The model was developed for the electrochemical arrangement shown in Figure 1 and described below. A 2 mm diameter disc electrode is positioned 180 μm ± 20 μm above a prism surface bearing the Ag nanoparticles and is used to generate the oxidant, $IrCl_6^{2-}$, from $IrCl_6^{3-}$, local to the surface. Experiments show that the Ag nanoparticles on the surface are highly dispersed, but as the interparticle spacing is much smaller than the electrode–prism separation, *d*, it is reasonable to treat the reactive prism surface as uniform (for the purpose of modeling) and diffusion between the electrode and prism as planar. The model considers the diffusion of the mediator within the thin layer cell coupled to the dissolution of the Ag layer at the prism boundary and calculates the absorbance of the Ag layer with time, as described later.

The Diffusional problem

The diffusion of species *i*, with concentration $c_i(z,t)$, in a one dimensional domain is given by

$$\frac{\partial c_i(z,t)}{\partial t} - D_i \frac{\partial^2 c_i(z,t)}{\partial z^2} = 0, \qquad (1)$$

for $z \in [0,d]$ where d is the distance between the prism and the electrode, and D_i is the diffusion coefficient of species *i* ($IrCl_6^{3-}$ or $IrCl_6^{2-}$). Assuming the $IrCl_6^{2-}$ can oxidize only the atoms on the surface of the nanoparticle, the boundary conditions for the reduced, $IrCl_6^{3-}$, and oxidized, $IrCl_6^{2-}$, forms of the mediator, denoted $c_R(z,t)$ and $c_O(z,t)$ respectively, in this case are given by

$$
\begin{aligned}
&c_{\mathrm{R}}(0,t)=0\\
&D_{\mathrm{O}}\frac{\partial c_{\mathrm{O}}}{\partial z}(0,t)=-D_{\mathrm{R}}\frac{\partial c_{\mathrm{R}}}{\partial z}(0,t)\\
&-D_{\mathrm{O}}\frac{\partial c_{\mathrm{O}}}{\partial z}(d,t)=D_{\mathrm{R}}\frac{\partial c_{\mathrm{R}}}{\partial z}(d,t)=kc_{\mathrm{O}}N_{\mathrm{NP}}A_{\mathrm{p}}(t)
\end{aligned}
\tag{2}
$$

for $0<t\le t_{\mathrm{step}}$, where t_{step} is the potential step time (the duration of the electrogeneration period) and

$$
\begin{aligned}
&c_{\mathrm{O}}(0,t)=0\\
&D_{\mathrm{O}}\frac{\partial c_{\mathrm{O}}}{\partial z}(0,t)=-D_{\mathrm{R}}\frac{\partial c_{\mathrm{R}}}{\partial z}(0,t)\\
&-D_{\mathrm{O}}\frac{\partial c_{\mathrm{O}}}{\partial z}(d,t)=D_{\mathrm{R}}\frac{\partial c_{\mathrm{R}}}{\partial z}(d,t)=kc_{\mathrm{O}}N_{\mathrm{NP}}A_{\mathrm{p}}(t)
\end{aligned}
\tag{3}
$$

for $t_{\mathrm{step}}<t$. Here k is the Ag dissolution rate constant, N_{NP} is the nanoparticle surface concentration (in mol cm^{-2}) on the prism and $A_{\mathrm{p}}(t)$ is the surface area of a nanoparticle which decreases as the nanoparticle is dissolved. Our focus is on initial rate measurements which allow us to neglect the small build up of Ag^{+} that will occur in the thin layer cell during the dissolution process. Additionally, because the change in particle size during dissolution is small, the rate constant was assumed to be independent of the nanoparticle size. These boundary conditions were coupled to an ordinary differential equation for $A_{\mathrm{p}}(t)$ describing the dissolution of Ag at the prism surface

$$
\frac{dA_{\mathrm{p}}(t)}{dt}=-\frac{4M\pi^{\frac{1}{2}}}{3\rho}kc_{\mathrm{O}}(d,t)\left(A_{\mathrm{p}}(t)\right)^{\frac{1}{2}},
\tag{4}
$$

where ρ is the density of Ag (10.5 g cm^{-3}) and M is the molecular weight of Ag (107.67 g mol^{-1}). The initial values for $A_{\mathrm{p}}(t)$ were obtained from the nanoparticle size determined by tapping mode Atomic Force Microscopy (TM-AFM).

Due to mass conservation of the redox couple within the thin layer cell and the equality of the diffusion coefficients of the oxidized and reduced forms of the mediator, the concentrations at any point are related by

$$c_R + c_O = c_R^*, \quad (5)$$

where c_R^* is the original bulk concentration of $IrCl_6^{3-}$. Thus, it is only necessary to solve the diffusion equation numerically for either c_O or c_R and $A_p(t)$.

Modeling changes in interfacial absorbance

To compute the interfacial absorbance with time the average nanoparticle size obtained by TM-AFM measurements was considered. The initial Ag nanoparticle surface concentration is known from TM-AFM measurements and the change in nanoparticle size with time was computed from the flux at the interface (equation 2, 3 and 4) assuming fcc packing of the atoms within the nanoparticles. The size-dependence of the absorbance was obtained from the experimental data of Cottancin *et al.*[35] which gives the absorption coefficient for nanoparticles of diameters in the range of 1.5 nm to 6.7 nm (4 nanoparticle sizes), for which there is a linear relationship of the absorption coefficient and nanoparticle diameter. As shown later, the extinction coefficient, ε_m, of Ag nanoparticles can be derived using this UV-vis data, TM-AFM and EW-CRDS measurements. With knowledge of the extinction coefficient and the data of Cottancin *et al.*, the size-dependent absorbance $A(a)$ can be estimated.

With A established, the best fit to the data was found by varying k. (6)

Experimental Section

Chemicals

Silver nitrate salt (stored in the dark), tribasic sodium citrate, sodium borohydrate, methanol (Aldrich, spectroscopy grade), PLL (MW 30000 – 70000, Sigma) were used as received.

Synthesis of Ag nanoparticles and sample preparation

Citrate-stabilized Ag nanoparticles were prepared following established methods.[34] In order to obtain colloids with a narrow size distribution, it was crucial to rinse all glassware with copious amounts of purified water from a Millipore Milli-Q system (resistivity > 18 MΩ cm) prior the sample preparation. 0.6 cm^3 of 0.1 M sodium borohydrate was added to 20 cm^3 of a solution containing equal concentrations (0.25 mM) of sodium citrate and Ag nitrate under strong stirring. The reaction was complete after two hours at room temperature.

The coverage and size distribution of nanoparticles achieved with deposition from quiescent solution onto PLL-functionalized silica surfaces was investigated by TM-AFM of PLL-coated quartz slides. Quartz slides were ashed in oxygen plasma for 1 min at 100 W (Emitech, K1050X) and wiped with methanol. PLL films were deposited from 1 mg cm^{-3} stock solution of the polyelectrolyte at pH 7. The quartz slides were then rinsed with ultrapure water and dried in an air flow. Ag nanoparticles were electrostatically adsorbed by exposing a PLL-modified quartz slide in a Ag nanoparticle solution for a defined time. For all TM-AFM measurements a Digital Instruments multimode atomic force microscope with a Nanoscope IIIa controller (Veeco, U.S.A.) was employed. Commercially available SPIP™ software was used for statistical grain analysis in order to obtain the size and the size distribution of the Ag nanoparticles.

EW-CRDS apparatus

The specifications of the CRD spectrometer used in this work (and the alignment procedure) was similar to that described elsewhere[32,36] and is shown in Figure 1a. The interface of interest was the

hypotenuse of a right angled prism which forms one optical element of a high finesse ring cavity. The remainder of the optical cavity consisted of two high-reflectance concave mirrors (*R* 99.997% at 405 nm, Los Gatos Research) with radii of curvature of 1 m. The other two surfaces of the fused silica prism (CVI) were coated with a standard antireflection coating (AR, R <0.5%, λ = 350-532 nm for normal incidence). The total length of the cavity was 58 cm and, at the geometry used, the penetration depth of the evanescent field was calculated to be 113 nm.[37] The cavity was filled by light from a pulsed diode laser (Power Technology Inc., 405 nm, 50 mW maximum output) operating at 5 kHz (TTI pulse generator, TGP110). Light intensity leaking out of the cavity due to reflection at the incident prism surface was measured with a photomultiplier tube (Electron Tubes, 9781B). The decay in the light level within the cavity was recorded on a 12-bit 400 MS/s oscilloscope card (Gage CS12400), analyzed using the fast Fourier transform method in order to extract the ring-down time.[38] For the purposes of plotting, the data were smoothed using a 25-point adjacent average. The ring-down time is characteristic of all optical losses within the cavity and from it the interfacial absorbance per pass within the evanescent field can be calculated in a straightforward manner.[36] Electrochemical data could be recorded along with the EW-CRDS response using a National Instruments PCI-6221 card. Custom-written LabVIEW software ensured optimal data synchronization. The same cell as described in reference [36] was employed for all EW-CRDS measurements.

Ultraviolet-visible (UV-vis) absorption spectroscopy

UV-vis absorption spectra were measured with a Lambda 25 UV-vis spectrometer (Perkin-Elmer Instruments).

Ag nanoparticle adsorption

0.2 cm^3 of PLL (1 mg cm^{-3} in ultra pure water) was contacted for 20 min with clean fused silica prisms, leading to PLL deposition by drop coating. After deposition, the prism was rinsed with ultrapure water and dried in a flow of air. The adsorption behavior of Ag nanoparticles, at different

dilutions, on PLL-modified fused silica prisms was followed by EW-CRDS in a similar way to that described previously for other metal nanoparticles.[32] In brief, 0.2 cm^3 of Ag colloid solution was injected into the cell above the substrate and the EW-CRDS response for the adsorption process was monitored continuously. Where the modified substrate was used for subsequent dissolution studies, adsorption was stopped after a defined time (typically 2 min) by removing the remaining colloidal solution and rinsing 5 times with 1.5 cm^3 ultrapure water. By this stage, a disperse film of nanoparticles had been deposited for which the surface coverage was known. The same procedure was followed prior to all dissolution experiments. After each experiment, the prism surface was wiped several times with methanol and ashed for 1 min in an O_2 plasma at 100 W. Ashing for such short times did not effect the properties of the prism and the initial ring-down time was always re-established.

Chronoamperometric EW-CRDS

As displayed in Figure 1b, the working electrode (2.0-mm-diameter circular platinum electrode with an overall diameter, including insulation, of 6.35 mm) was placed over the region of the prism co-incident with the evanescent field using a 3-axis micropositioner in such a way as to create a thin-layer electrochemical cell. The distance between the working electrode and the prism surface was chosen to be 200 μm – well outside the evanescent field – and the electrode itself did not affect the EW-CRDS signal. Two Pt wires acted as counter and quasi-reference electrodes, respectively, with all potentials applied with respect to the latter. Measurements were made with a homebuilt potentiostat controlled by a National Instruments card (NI PCI-6221) for potential control and data acquisition. The dissolution of the nanoparticles was induced by oxidizing 1 mM or 0.1 mM $IrCl_6^{3-}$ in 0.1 M KNO_3 supporting electrolyte. The potential was stepped from -0.1 V to +0.4 V for a defined time during which the oxidation of $IrCl_6^{3-}$ to $IrCl_6^{2-}$ was diffusion-controlled. The potential was then returned to -0.1 V where $IrCl_6^{2-}$ was reduced back to $IrCl_6^{3-}$.

Flow EW-CRDS

Micropipettes with a typical internal diameter of 300 μm were produced by pulling a 2-mm-o.d. borosilicate glass capillary (Harvard Apparatus, UK) using a PB7 Narishighe micropipette puller and cutting the tapered the end with a sharp scalpel. The resulting nozzle was polished using a home-built polishing wheel with a 0.1-μm diamond polishing pad (Buehler, USA). The micropipette was placed over the region of the evanescent field using a 3-axis micropositioner at a distance of *ca.* 500 μm from the prism surface (Figure 1c). Flow of the solution of K_2IrCl_6 at concentrations between 1 μM and 5 μM at a constant rate was achieved with a syringe pump (KDS100, KD Scientific) equipped with a 10 cm^3 glass syringe (Hamilton). The system delivered flow rates in the range of 0.22 – 35.1 μL s^{-1}. Typical flow rates used were between 1.7 and 33.3 μL s^{-1}. All solutions were freshly prepared immediately prior to experiments.

Results and discussion

TM-AFM

Figure 2 shows a typical 1 μm x 1 μm TM-AFM height image of Ag nanoparticles on a PLL modified fused silica slide following adsorption from stock solution. A clear submonolayer coverage of Ag nanoparticles is evident, from which their size, the size distribution and the coverage of the nanoparticles can be estimated. The average size of the Ag nanoparticles was found to be 7.6 nm ± 2.6 nm and in this case the coverage was 60 ± 17 nanoparticles per μm^{-2}. As shown below, there is excellent agreement between surface coverages measured by TM-AFM and EW-CRDS.

Ag nanoparticle adsorption

The concentration of Ag nanoparticles in solution obtained from the synthesis can be estimated assuming that all Ag^+ ions present in the solution reacted to Ag^0. Using equation 5, the nanoparticle concentration is given by[39]

$$c_{\mathrm{NP}} = \frac{c_{\mathrm{Ag^+}}}{\sum f_i \frac{N_A}{M} \rho V_{\mathrm{NP}}} \tag{7}$$

where $c_{\mathrm{Ag+}}$ is the initial concentration of Ag^+ (0.25 mM), f_i is the frequency of nanoparticles with radius a_i as obtained by TM-AFM, N_A is Avogadro's constant and V_{NP} is the volume of nanoparticles with radius a_i. The distribution is normalized so that it satisfies

$$\sum_{i=1}^{L} f_i = 1 \tag{8}$$

In this work, the resulting concentration was calculated to be 11.3 nmol dm^{-3}. With this information, the extinction coefficient of the Ag nanoparticle solution can be calculated by plotting the relative peak absorbance of different dilutions from UV-vis spectroscopy as a function of concentration (see Figure 3). As shown in the inset of Figure 3, the relative absorption values show a good linear dependence on the concentration. The calculated molar extinction coefficient for Ag nanoparticles was $\varepsilon_m = 2.88 \times 10^{11}$ cm^2 mol^{-1}, which is in good agreement with previous reports.[39]

The time-dependent surface concentration could be calculated using absorbance values measured from the EW-CRDS data, $A(t)$, and the extinction coefficient:

$$N_{\mathrm{NP}}(t) = \frac{A(t)}{\varepsilon_m}. \tag{9}$$

This equation is valid only if there is negligible absorbance from the bulk solution within the evanescent field. Our simulations support this assumption: even assuming a 500 μm effective thickness, simulations show that the bulk absorbance never exceeds 3% of the interfacial absorbance for any of the results reported here.

For a typical absorbance value of 0.002, the corresponding calculated surface coverage was 42 μm^{-2} which is similar to the value of 60 ± 17 nanoparticles per μm^{-2} obtained by TM-AFM measurements for the Ag nanoparticle adsorption from the stock solution. This represents an effective surface coverage of *ca.* 0.2 %. This also suggests that the extinction coefficient for Ag

nanoparticles adsorbed on the surface is very similar to that in bulk solution measured by UV-vis spectroscopy.

Figure 4 shows the time-dependence of the interfacial absorbance as Ag nanoparticles adsorb irreversibly on the PLL-modified fused silica. As the figure shows, the experimental absorbance data fit satisfactorily to a simple square root dependence ($t^{1/2}$) which is expected for diffusion-controlled adsorption.[40] Since the adsorption process is completely diffusion-controlled, the diffusion coefficient of Ag nanoparticles, D_{NP} , can be calculated[41] using

$$A(t) = 2\varepsilon c_{NP} \pi^{-1/2} D_{NP}^{1/2} t^{1/2} , \quad (10)$$

where $A(t)$ represents the time-dependent optical absorption, which relates to the amount adsorbed on the surface. The diffusion coefficient was calculated to be (1.92 ± 0.22) x 10^{-6} cm^2 s^{-1} using all the sets of data in Figure 4. This value should be treated as an upper limit since we make no attempt to account for the effects of natural convection which could be significant especially at later time.

The fact that the adsorption of nanoparticles can be followed from a solution that contains such a low concentration of Ag nanoparticles is testament to the sensitivity of EW-CRDS, coupled with the strength of the localized surface plasmon peak of Ag nanoparticles which enables the detection of very low coverages of nanoparticles. As shown in Figure 4, a dilution of the stock solution of 1:100 (*i.e.,*. 0.18 nmol dm^{-3}) gives rise to an absorbance value of 0.00045 after 120 s, which corresponds to only 18 particles per μm^{-2}. For the dissolution experiments which follow, surfaces were prepared from either the 1:20 or the 1:100 dilutions. The adsorption was typically stopped after *ca.* 120 s. The corresponding absorbance value of the transient at this time was used to determine the surface coverage of Ag nanoparticles.

Electrochemical dissolution

The electrochemical dissolution of Ag nanoparticles can be summarized by the following redox reaction:

$$IrCl_6^{2-} + Ag(0) \rightarrow IrCl_6^{3-} + Ag(I) \quad (11)$$

In these experiments, $IrCl_6^{2-}$ was electrogenerated from $IrCl_6^{3-}$ at an electrode situated *ca.* 200 μm above the prism surface. The electrogeneration process occurred for a defined time before the potential of the working electrode was switched back to a value which reduced $IrCl_6^{2-}$ to $IrCl_6^{3-}$. The current-time behavior displayed a Cottrellian response. Figure 5a and b show typical experimental EW-CRDS transients for the electrochemical dissolution process for two different step times of 5 s (a) and 10 s (b), together with simulated transients using the model outlined earlier. The dissolution rate constant per nanoparticle, *k*, was calculated to be 3.0×10^{-3} cm s^{-1} for the 5 s step and 2.5×10^{-3} cm s^{-1} for the 10 s step.

After an initial delay period of a few seconds, during which $IrCl_6^{2-}$ diffuses from the electrode towards the prism, the interfacial absorbance slowly decreases with time. This can be attributed to the dissolution of Ag nanoparticles within the evanescent field. Since the plasmon resonance of the Ag nanoparticles is the main contribution to the extinction at 405 nm, the decrease in the absorbance due to the dissolution process will be determined by the number of particles within the evanescent field as well as their size.

Figure 6 shows the absorbance transient for a potential step time of 600 s but at a lower $IrCl_6^{3-}$ concentration of 0.1 mM. The absorbance decreases much more gradually for this low concentration which can be explained by the fact that the dissolution process is limited with the amount of $IrCl_6^{2-}$ present in the thin layer cell. The rate constant, *k*, for this transient was determined to be 2.5×10^{-3} cm s^{-1}, which is in very good agreement with the rate constants obtained above. The mean rate constant for the dissolution per nanoparticle from several runs was calculated to be $(2.6 \pm 0.6) \times 10^{-3}$ cm s^{-1}.

Convective Dissolution

An alternative strategy to investigate the dissolution behavior of Ag nanoparticles was to introduce a micropipette close to the prism surface through which $IrCl_6^{2-}$ was directly injected onto the colloidal particles. Figure 7a shows the concentration dependence of the dissolution rate for a

constant flow rate of 8.3 μL s^{-1} in which all transients have been normalized with respect to their initial absorbance:

$$A_{rel} = \frac{A_{exp}(t)}{A(t=0)}, \quad (12)$$

where A_{exp} is the absorbance transient and A_{ini} the interfacial absorbance of Ag nanoparticles before dissolution begins. The sensitivity of this approach, with a constant supply of $IrCl_6^{2-}$ even at very low concentrations of $IrCl_6^{2-}$ is clear. Experiments at higher $IrCl_6^{2-}$ concentrations demonstrated complete dissolution of the nanoparticles.

Studies at different flow rates of $IrCl_6^{2-}$ solution were also carried out and the results are displayed in Figure 7b. Higher flow rates lead to faster dissolution, indicating at least partial control of the kinetics by mass transport of $IrCl_6^{2-}$ to the surface. For future studies, we plan to establish a finite element model, building on to earlier investigations[42] in order to describe this type of hydrodynamic system more rigorously.

Conclusions

The time-dependent adsorption of Ag nanoparticles on PLL-modified silica and the corresponding surface coverage has been measured accurately using EW-CRDS. This technique has proven very useful as a detection tool for very low surface concentrations of Ag nanoparticles (typically 20-60 particles per μm^{-2}). Additionally, EW-CRDS has been applied successfully to study the chemical kinetics of nanoparticle oxidative dissolution. This sensitive technique has been coupled with two complementary approaches to dissolve immobilized colloidal particles on functionalized surfaces: electrochemical dissolution via a redox mediator; and convective dissolution using a microcapillary setup to deliver the oxidant. The heterogeneous rate constant for dissolution was established as 2.6×10^{-3} cm s^{-1}. These measurements illustrate the ability of EW-CRDS to obtain kinetic information; especially on inert supporting surfaces such as silica or polymer-modified silica which are traditionally challenging to study. The combination of EW-CRDS with both chronoamperometric

and flow methods show that the dissolution process can be monitored even with very low fluxes and low concentrations of reagents, making both approaches excellent tools for potential sensing applications.

Acknowledgements

This work was generously supported by the Engineering and Physical Sciences Research Council under grant EP/C00907X. HVP is grateful for a studentship under the MOAC doctoral training centre and SRM is further grateful to the EPSRC for his Advanced Research Fellowship. MZ gratefully acknowledges a Marie Curie Incoming International Fellowship (040126).

Figures captions

Figure 1: a) Experimental arrangement for the study of silver nanoparticle dissolution using evanescent wave cavity ring-down spectroscopy. Home-synthesized silver nanoparticles are immobilized on the PLL-functionalized hypotenuse of a fused silica prism which forms one element of an optical ring cavity. In b) $IrCl_6^{2-}$ is electrogenerated from $IrCl_6^{3-}$ in an axisymmetric thin layer electrochemical cell, whilst in c) $IrCl_6^{2-}$ solution is injected in close proximity to the surface *via* a 300 μm diameter micropipette.

Figure 2: Top: Representative 1 x 1 μm tapping mode AFM image of Ag nanoparticles on PLL modified quartz following adsorption for 2 min. Bottom: Statistical analysis of particle size from which a mean particle size of 7.6 nm ± 2.6 nm was obtained from several images.

Figure 3: Bulk UV-visible absorbance spectra for different dilutions of Ag nanoparticles in water. The large band at 400 nm corresponds to the localized surface plasmon resonance band of Ag. Inset: Peak absorbance *versus* colloid concentration.

Figure 4: Interfacial absorbance transients for the adsorption of several dilutions of nanoparticles on PLL modified fused silica. The dilutions are: 1:10, 1:20, 1:30, 1:50 and 1:100. The red lines denote fits assuming diffusion-controlled ($\propto t^{1/2}$) adsorption kinetics.

Figure 5: Interfacial absorbance transients for the electrochemical dissolution of Ag nanoparticles using 1 mM $IrCl_6^{3-}$ oxidized for 5 s (a) and 10 s (b) at the electrode. The red lines indicate fits obtained using the model described in the text from which rate constants for the dissolution of 3.0×10^{-3} cm s^{-1} for the 5 s potential step and 2.5×10^{-3} cm s^{-1} for the 10 s potential step were extracted.

Figure 6: Interfacial absorbance transient for the electrochemical dissolution of Ag nanoparticles using 0.1 mM $IrCl_6^{3-}$ oxidized for 600 s. The red line indicates a fit obtained using the model described in the text from which rate constant for the dissolution of 2.5×10^{-3} cm s^{-1} was extracted.

Figure 7: (a): Interfacial absorbance transients showing the dissolution of Ag nanoparticles using the micropipette setup with $IrCl_6^{2-}$ solution concentrations of A) 0.1 µM, B) 0.5 µM, C) 1 µM. A constant flow of $IrCl_6^{2-}$, 16.6 µL s^{-1}, was used for all measurements. (b): Dissolution of Ag nanoparticles using the micropipette setup with 1µM $IrCl_6^{2-}$ solution flow rates of A) 1.7 µL s^{-1}, B) 8.3 µL s^{-1}, C) 33.3 µL s^{-1}.

Figure 1

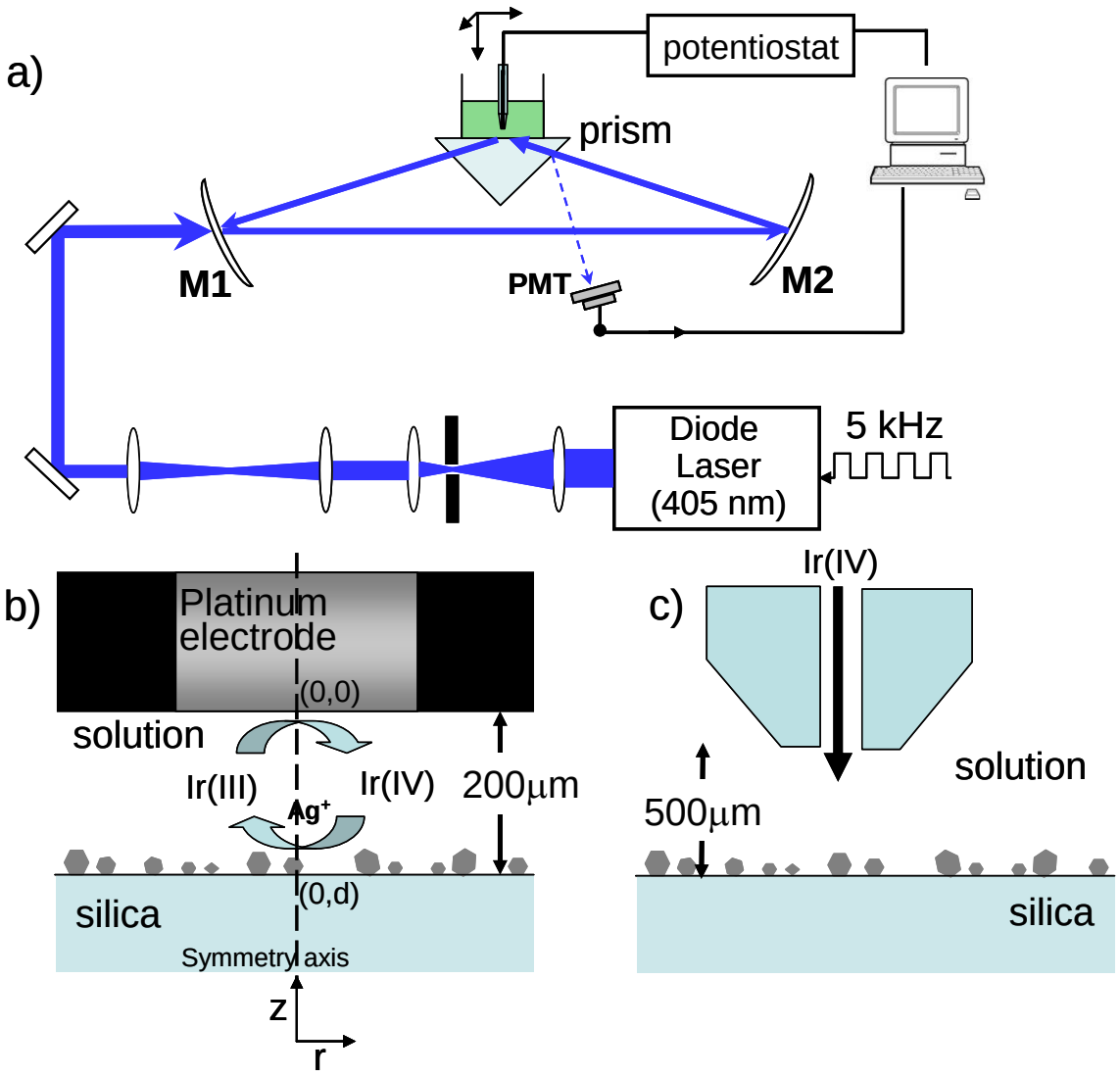
a)
potentiostat
prism
M1
PMT
M2
Diode
Laser
(405 nm)
5 kHz
b)
Platinum
electrode
(0,0)
solution
Ir(III)
Ir(IV)
200μm
Ag+
(0,d)
silica
Symmetry axis
z
r
c)
Ir(IV)
solution
500μm
silica

Figure 2

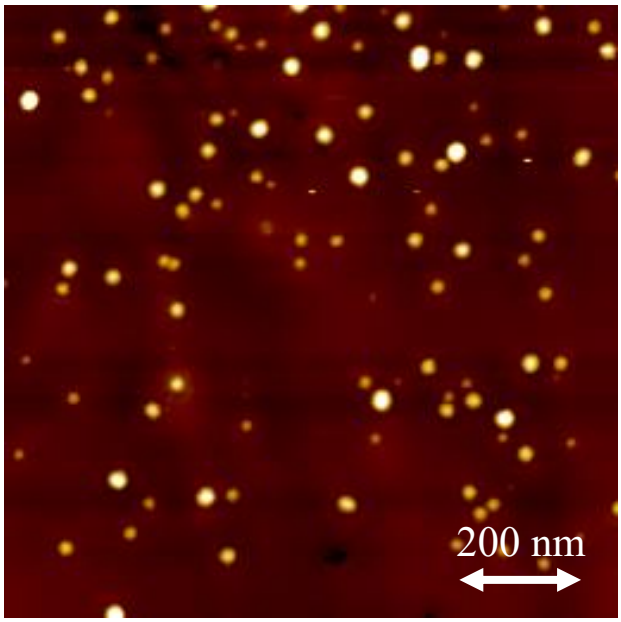
200 nm

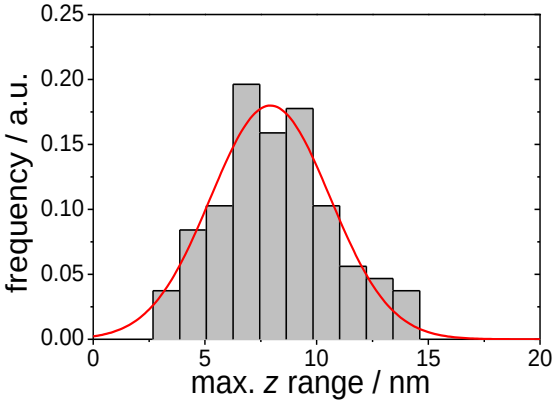
frequency / a.u.
0.25
0.20
0.15
0.10
0.05
0.00
0
5
10
15
20
max. z range / nm

Figure 3

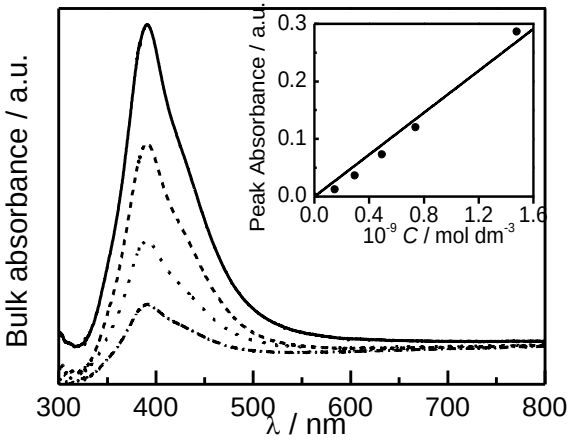
Bulk absorbance / a.u.
λ / nm
300
400
500
600
700
800
Peak Absorbance / a.u.
0.0
0.1
0.2
0.3
0.0
0.4
0.8
1.2
1.6
10-9 C / mol dm-3

Figure 4

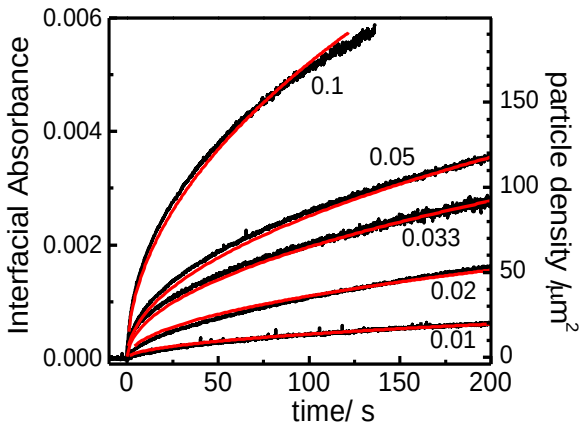
0.006
0.004
0.002
0.000
Interfacial Absorbance
0
50
100
150
200
time/ s
150
100
50
0
particle density /μm²
0.1
0.05
0.033
0.02
0.01

Figure 5

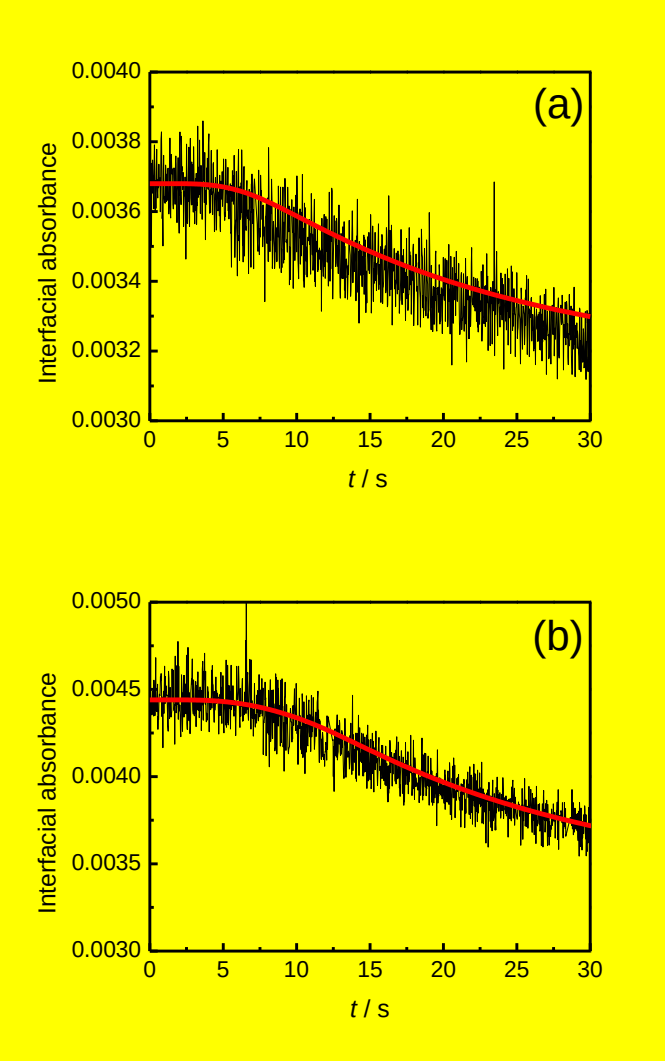
(a)
Interfacial absorbance
0.0040
0.0038
0.0036
0.0034
0.0032
0.0030
0
5
10
15
20
25
30
t / s
(b)
Interfacial absorbance
0.0050
0.0045
0.0040
0.0035
0.0030
0
5
10
15
20
25
30
t / s

Figure 6

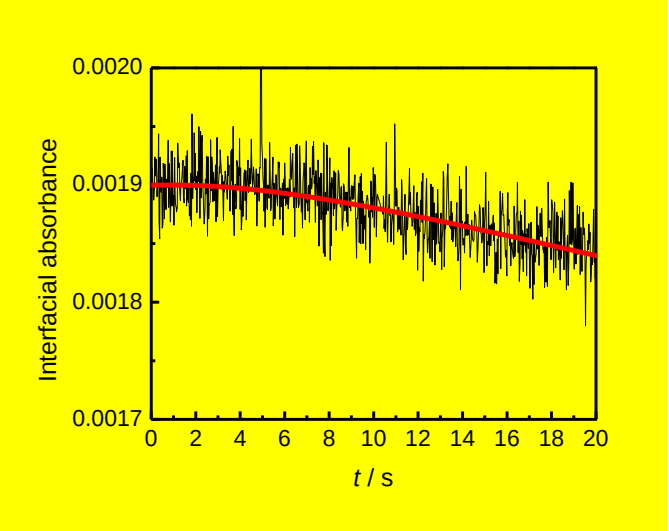
0.0020
0.0019
0.0018
0.0017
Interfacial absorbance
0
2
4
6
8
10
12
14
16
18
20
t / s

Figure 7a and 7b

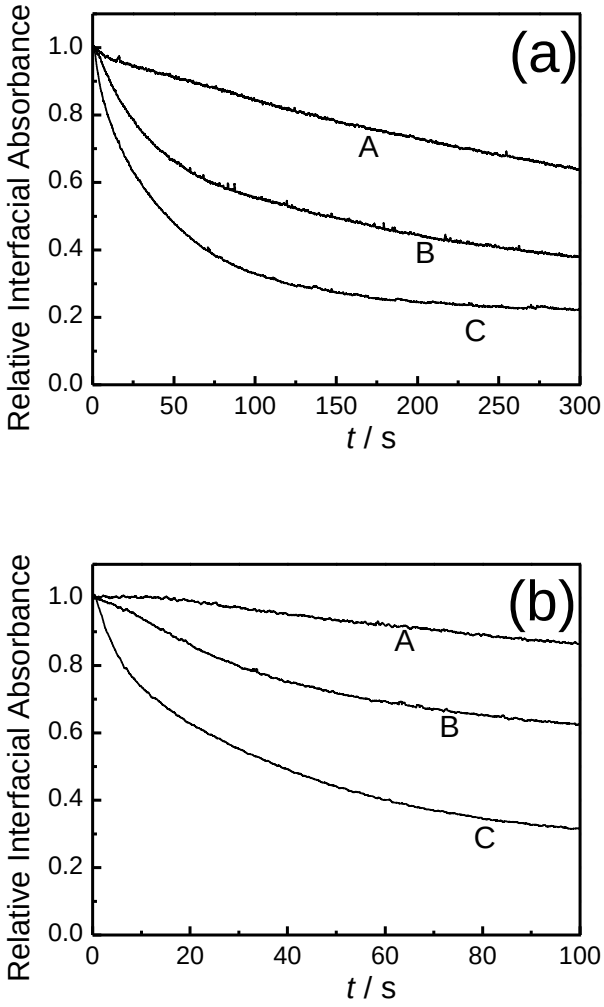

References

(1) Bonnemann, H.; Richards, R. M. *Eur. J. Inorg. Chem.* **2001**, 2455.
(2) Gittins, D. I.; Bethell, D.; Schiffrin, D. J.; Nichols, R. J. *Nature* **2000**, *408*, 67.
(3) Shipway, A. N.; Katz, E.; Willner, I. *ChemPhysChem* **2000**, *1*, 18.
(4) Bauer, G.; Pittner, F.; Schalkhammer, T. *Mikrochim. Acta* **1999**, *131*, 107.
(5) Habicht, W.; Behrens, S.; Wu, J.; Unger, E.; Dinjus, E. *Surf. Interface Anal.* **2004**, *36*, 720.
(6) Kohut, A.; Voronov, A.; Peukert, W. *Part. Part. Syst. Char.* **2006**, *22*, 329.
(7) Lu, H. C.; Yi, G. S.; Zhao, S. Y.; Chen, D. P.; Guo, L. H.; Cheng, J. *J. Mater. Chem.* **2004**, *14*, 1336.
(8) Maxwell, D. J.; Taylor, J. R.; Nie, S. M. *J. Am. Chem. Soc.* **2002**, *124*, 9606.
(9) Lee, J. S.; Lytton-Jean, A. K. R.; Hurst, S. J.; Mirkin, C. A. *Nano Lett.* **2007**, *7*, 2112.
(10) Liu, T.; Zhong, J.; Gan, X.; Fan, C. H.; Li, G. X.; Matsuda, N. *ChemPhysChem* **2003**, *4*, 1364.
(11) Chen, Y. C.; Young, R. J.; Macpherson, J. V.; Wilson, N. R. *J. Phys. Chem. C* **2007**, *111*, 16167.
(12) Li, X. L.; Xu, W. Q.; Zhang, J. H.; Jia, H. Y.; Yang, B.; Zhao, B.; Li, B. F.; Ozaki, Y. *Langmuir* **2004**, *20*, 1298.
(13) Doering, W. E.; Nie, S. M. *J. Phys. Chem. B* **2002**, *106*, 311.
(14) Macpherson, J. V.; Slevin, C. J.; Unwin, P. R. *J. Chem. Soc., Faraday Trans.* **1996**, *92*, 3799.
(15) Meulenkamp, E. A. *J. Phys. Chem. B* **1998**, *102*, 7764.
(16) Rimer, J. D.; Trofymluk, O.; Navrotsky, A.; Lobo, R. F.; Vlachos, D. G. *Chem. Mater.* **2007**, *19*, 4189.
(17) Shi, H. Z.; Bi, H. J.; Yao, B. D.; Zhang, L. D. *Appl. Surf. Sci.* **2000**, *161*, 276.
(18) Pal, T.; Sau, T. K.; Jana, N. R. *Langmuir* **1997**, *13*, 1481.
(19) Chen, S. H.; Akai, T.; Kadono, K.; Yazawa, T. *Appl. Phys. Lett.* **2001**, *79*, 3687.
(20) Jiang, X. W.; Qiu, J. R.; Zeng, H. D.; Zhu, C. S.; Hirao, K. *Chem. Phys. Lett.* **2004**, *391*, 91.
(21) Carvalho, I. C. S.; Mezzapesa, F. P.; Kazansk, P. G.; DepariS, O.; Kawazu, M.; Sakaguchi, K. *Mater. Sci. Eng., C* **2007**, *27*, 1313.
(22) Podlipensky, A.; Abdolvand, A.; Seifert, G.; Graener, H.; Deparis, O.; Kazansky, P. G. *J. Phys. Chem. B* **2004**, *108*, 17699.
(23) Zhang, M. Q.; Wittstock, G.; Shao, Y. H.; Girault, H. H. *Anal. Chem.* **2007**, *79*, 4833.
(24) Zhang, M.; Becue, A.; Prudent, M.; Champod, C.; Girault, H. H. *Chem. Commun.* **2007**, 3948.
(25) Rodriguez-Sanchez, M. L.; Rodriguez, M. J.; Blanco, M. C.; Rivas, J.; Lopez-Quintela, M. A. *J. Phys. Chem. B* **2005**, *109*, 1183.
(26) Fan, H. F.; Li, F.; Zare, R. N.; Lin, K. C. *Anal. Chem.* **2007**.
(27) Fisk, J. D.; Batten, R.; Jones, G.; O'Reilly, J. P.; Shaw, A. M. *J. Phys. Chem. B* **2005**, *109*, 14475.
(28) Everest, M. A.; Black, V. M.; Haehlen, A. S.; Haveman, G. A.; Kliewer, C. J.; Neill, H. A. *J. Phys. Chem. B* **2006**, *110*, 19461.
(29) Fan, H. F.; Hung, C. Y.; Lin, K. C. *Anal. Chem.* **2006**, *78*, 3583.
(30) Hallock, A. J.; Berman, E. S. F.; Zare, R. N. *Anal. Chem.* **2002**, *74*, 1741.
(31) Pipino, A. C. R.; Hudgens, J. W.; Huie, R. E. *Chem. Phys. Lett.* **1997**, *280*, 104.
(32) Mazurenka, M.; Hamilton, S. M.; Unwin, P. R.; Mackenzie, S. R. *J. Phys. Chem. C* **2008**, *112*, 6462.
(33) Decher, G. *Science* **1997**, *277*, 1232.
(34) Schnippering, M.; Carrara, M.; Foelske, A.; Kotz, R.; Fermin, D. J. *Phys. Chem. Chem. Phys.* **2007**, *9*, 725.
(35) Cottancin, E.; Celep, G.; Lerme, J.; Pellarin, M.; Huntzinger, J. R.; Vialle, J. L.; Broyer, M. *Theor. Chem. Acc.* **2006**, *116*, 514.
(36) Mazurenka, M.; Wilkins, L.; Macpherson, J. V.; Unwin, P. R.; Mackenzie, S. R. *Anal. Chem.* **2006**, *78*, 6833.
(37) de Fornel, F. *Evanescent Waves: From Newtonian Optics to Atomic Optics*; Springer-Verlag: Berlin, 1997.
(38) Mazurenka, M.; Wada, R.; Shillings, A. J. L.; Butler, T. J. A.; Beames, J. M.; Orr-Ewing, A. J. *Appl. Phys. B: Lasers Opt.* **2005**, *81*, 135.
(39) Liu, X. O.; Atwater, M.; Wang, J. H.; Huo, Q. *Colloids Surf., B* **2007**, *58*, 3.
(40) Crank, J. *The Mathematics of Diffusion*; Oxford University Press: Oxford, 1975.
(41) Adamczyk, Z. *J. Colloid Interface Sci.* **2000**, *229*, 477.
(42) Bitziou, E.; Rudd, N. C.; Edwards, M. A.; Unwin, P. R. *Anal. Chem.* **2006**, *78*, 1435.